

Photoproduction of $\gamma p \rightarrow K^+ \Lambda^*(1520)$ and decay of $\Lambda^*(1520) \rightarrow K^- p$ in the Reggeized framework

Byung-Geel Yu* and Kook-Jin Kong†

Research Institute of Basic Sciences, Korea Aerospace University, Goyang, 10540, Korea

(Dated: September 11, 2018)

Photoproduction of the $\Lambda^*(1520)$ resonance of spin-parity $\frac{3}{2}^-$ off the proton target is investigated within the Regge framework where the t -channel reggeization is applied for the $K(494) + K^*(892) + K_2^*(1430)$ exchanges in the Born amplitude. The present model is based on the two basic ingredients; the one is the minimal gauge prescription for the convergence of the reaction and the other is the role of the K_2^* crucial to be consistent with high energy data. The cross sections for the total, differential and photon polarization asymmetry are reproduced without fit parameters and compared with existing data. The LAMP2 and LEPS measurements of the angular distribution of the K^- in the $\Lambda^*(1520) \rightarrow K^- p$ decay are investigated and found to be dominated by the decay of Λ^* with helicity $\pm 3/2$ based on the analysis of the density matrix elements related. Detailed discussion on the density matrix elements is given to clarify the analysis of the observable. The reaction mechanism is featured by the dominance of the contact term with the K and K_2^* exchanges following in the low energy region. The K^* exchange appears in minor role. At high energies beyond $E_\gamma \approx 5$ GeV the role of K_2^* exchange leads over other exchanges in the reaction process.

PACS numbers: 25.20.Lj, 11.55.Jy, 13.60.Rj, 13.60.Le, 14.40.Df

Keywords: $\Lambda(1520)$ photoproduction, spin 3/2 resonance, Regge trajectory, tensor meson exchange, density matrix elements

I. INTRODUCTION

To study electromagnetic production of strangeness from a nucleon is important in hadron physics because it provides information about the interaction between nucleon and hyperon as well as the static properties of hyperon. There has been a growth of empirical data dedicated to the study of the hyperons and their resonances produced by hadronic and electromagnetic probes.

Of these, the reaction $\gamma p \rightarrow K^+ \Lambda^*(1520)$ is an interesting process in both sides of theory and experiment because the reaction process involves the production of the negative-parity hyperon-resonance of spin-3/2 via the process $\gamma p \rightarrow K^+ K^- p$.

Given the empirical data recently measured with accuracy from the CLAS [1], LEPS [2, 3], and SAPHIR [4] Collaborations up to photon energy $E_\gamma = 3$ GeV, besides the old measurements from the LAMP2 group at higher energies $E_\gamma = 2.8 - 4.8$ GeV [5], and 11 GeV at the SLAC [6], theoretical efforts on the reaction process have been made to investigate the production mechanism based on the effective Lagrangian approach [7], or on a sort of the hybrid model using the t -channel Regge-pole interpolated with the Feynman propagator [8].

To unravel the role of the baryon resonances in the low energy region the latter approach was more elaborated to calculate the contributions of baryon resonances [9–11]. In these studies the contributions of the K and K^* in the t -channel exchange are analyzed and the role of the $N^*(2120)$ [previously called $D_{13}(2080)$] is identified in

the resonance region.

On the other hand, it has been an issue to determine the $K^* N \Lambda^*$ coupling constant from the present process because it could give a hint on our understanding of the structure of the Λ^* resonance. In Refs. [12, 13] the $\bar{K}N$ coupled-channel approach to the Λ^* leads to the coupling constant $g_{K^* N \Lambda^*} / m_{K^*} = 1.56 / m_{K^*}$, whereas the quark model predicts the value, i.e., $g_{K^* N \Lambda^*} \simeq 10$ much larger by an order of magnitude.

In recent experiments it has been another topic to measure the decay angular distribution of the K^- in the $\Lambda^*(1520) \rightarrow K^- p$ decay process, since the observable is expected to provide information about spin exchanges of K and K^* in understanding the production mechanism. Nevertheless, however, the interpretation of it seems not clear yet, because the recent data on the photoproduction [4] and the result from electroproduction process [14] lead to a conclusion contradictory to the LAMP2 data.

With these issues in mind, we, here, investigate the $\gamma p \rightarrow K^+ \Lambda^*(1520)$ process off the proton target from threshold to the photon energy 11 GeV, where there is a data point measured in the SLAC experiment [6]. Our purpose here is to provide a theoretical framework which can afford to describe the reaction without either fit-parameters or any modulation of the particle propagation for a convergence of the process at high energies. Indeed, the reaction with the Λ^* of spin-3/2 in the final state would give rise to a divergence as the photon energy increases. Nevertheless a special gauge prescription, the so-called the minimal gauge prescription, adopted in Refs. [15–17] simplifies the analysis of such reaction processes to a greater extent. This interesting result is a consequence of the Ward identity in the electromagnetic coupling vertex of the spin-3/2 baryon in the Rarita-Schwinger formalism [18], and supported further

* E-mail: bgyu@kau.ac.kr

† E-mail: kong@kau.ac.kr

by the agreements with high energy data of $\pi\Delta$ and $K\Sigma^*$ photoproductions.

We also point out the important role of the spin-2 tensor meson which is crucial to agree with existing data on $\gamma N \rightarrow K^+\Sigma^*(1385)$ as well as $\gamma p \rightarrow \pi^\pm\Delta(1232)$ at high energies [15, 17]. In this work we will consider the role of the tensor meson K_2^* with an expectation that the uncertainty in the role of the K^* arisen from the previous works [7, 8, 12, 13, 19] but unanswered yet can be resolved by considering the role of the K_2^* as a natural parity together with K^* .

This paper is organized as follows: In Sec. II, we provide a general formalism for the photoproduction amplitude with a brief introduction of the minimal gauge for the invariant K exchange. The coupling vertex for the $K_2^*p\Lambda^*$ is newly introduced with discussion on determining its coupling constants. Numerical results are given in Section III for the analyses of the old LAMP2/SLAC data and the recent CLAS/LEPS measurements. This will includes the cross sections for the total, differential, beam polarization asymmetry. Analysis of the decay angular distribution of K^- in the $\Lambda^* \rightarrow K^-p$ decay is given in detail based on the density matrix elements related. We give a summary and discussion in Section IV. The kinematics related to the t -channel helicity frame of the particle rest is defined in the Appendix A, and the angular distribution function in terms of the density matrix elements is given in the Appendix B.

II. PHOTOPRODUCTION AMPLITUDE IN THE MINIMAL GAUGE

We begin with the production amplitude for $\gamma(k) + p(p) \rightarrow K^+(q) + \Lambda^*(p')$ which is given by

$$i\mathcal{M} = i\mathcal{M}_K + i\mathcal{M}_{K^*} + i\mathcal{M}_{K_2^*}, \quad (1)$$

where each term represents the t -channel K , K^* , and K_2^* Regge-pole amplitude in order. The respective 4-momenta of the photon, proton, kaon, and Λ^* are denoted by k , p , q , and p' in Fig. 1 (a).

In these terms the latter two exchanges are themselves gauge invariant. However, the K exchange in the t -channel is not gauge invariant as expressed in the Born amplitude, i.e.,

$$iM_{t(K)} = e_K \frac{f_{KN\Lambda^*}}{m_K} \bar{u}_{\Lambda^*}^\nu(p') \gamma_5 Q_\nu \frac{2q \cdot \epsilon}{t - m_K^2} u_N(p), \quad (2)$$

where e_K is the kaon charge, ϵ is photon polarization, and $Q^\nu = (q - k)^\nu$ is the t -channel momentum transfer.

For the gauge invariant K exchange in Eq. (2) the current conservation following the charge conservation, $e_p - e_K - e_{\Lambda^*} = 0$, requires the inclusion of the charge term of the proton-pole in the s -channel and the contact term. Here, e_p and e_{Λ^*} are the respective charges of proton and Λ^* . Since the usual Dirac charge-coupling term in the proton-pole is, $e_p(\not{p} + \not{k} + M)\not{\epsilon} = e_p(2p \cdot \epsilon + \not{k}\not{\epsilon})$, it can be reduced to $e_p 2p \cdot \epsilon$ by removing the transverse

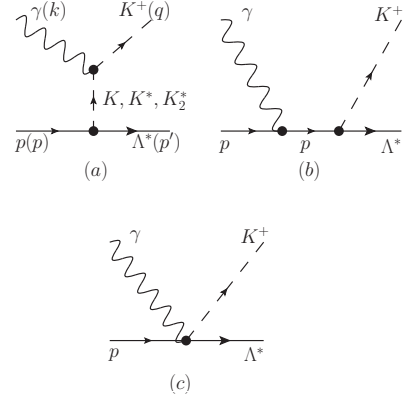


FIG. 1. Feynman diagrams for $\gamma p \rightarrow K^+\Lambda^*$. The exchange of K in the t -channel (a), the proton-pole in the s -channel (b), and the contact term (c) are the basic ingredients for gauge invariance of the reaction. The K^* and K_2^* exchanges in the t -channel (a) are themselves gauge-invariant.

term by redundancy with respect to gauge invariance in the sense of the minimal ¹ as discussed in Refs. [15, 17].

Thus, the gauge-invariant extension of the K exchange which is now Reggeized is given by

$$i\mathcal{M}_K = i [M_{t(K)} + M_{s(p)} + M_c] \times (t - m_K^2) \times \mathcal{R}^K(s, t) e^{-i\pi\alpha_K(t)}, \quad (3)$$

where

$$iM_{s(p)} = e_p \frac{f_{KN\Lambda^*}}{m_K} \bar{u}_{\Lambda^*}^\nu(p') \gamma_5 q_\nu \frac{2p \cdot \epsilon}{s - M_p^2} u_N(p), \quad (4)$$

$$iM_c = -e_K \frac{f_{KN\Lambda^*}}{m_K} \bar{u}_{\Lambda^*}^\nu(p') \gamma_5 \epsilon_\nu u_N(p), \quad (5)$$

are the proton-pole and the contact term, and

$$\mathcal{R}^\varphi(s, t) = \frac{\pi\alpha'_\varphi}{\Gamma[\alpha_\varphi(t) + 1 - J] \sin \pi\alpha_\varphi(t)} \left(\frac{s}{s_0}\right)^{\alpha_\varphi(t) - J} \quad (6)$$

is the Regge propagator written collectively for the $\varphi(=K, K^*, K_2^*)$ of spin- J . The $\alpha_\varphi(t)$ is the trajectory and $s_0 = 1 \text{ GeV}^2$ is taken as usual.

For the higher-spin meson exchanges we consider the vector-meson K^* and the Reggeized amplitude relevant to the leading contribution of the $K^*N\Lambda^*$ interaction is given by

$$i\mathcal{M}_{K^*} = -i \frac{g_{\gamma K K^*}}{m_0} \frac{f_{K^* N \Lambda^*}}{m_{K^*}} \epsilon^{\alpha\beta\lambda\sigma} \epsilon_\alpha k_\beta q_\lambda \times \bar{u}^\nu(p') (Q_\nu g_{\nu\sigma} - Q_\nu \gamma_\sigma) u(p) \mathcal{R}^{K^*}(s, t) e^{-i\pi\alpha_{K^*}(t)}, \quad (7)$$

¹ The minimal gauge requires the pure charge term of the proton-pole to be included. If one uses $e_p(\not{p} + \not{k} + M_p)\not{\epsilon}$ in Eq. (4), but still containing the transverse component, he/she cannot obtain an agreement with the cross section data without a cutoff function as shown in Fig. 2 (a) below.

with the mass parameter $m_0 = 1$ GeV.

In accordance with our previous work on $\gamma N \rightarrow K^+ \Sigma^*(1385)$, we introduce the tensor meson K_2^* exchange in the t -channel to the present reaction process. By considering the parity of the Λ^* opposite to the Σ^* the new Lagrangian for the $K_2^* N \Lambda^*$ coupling firstly considered in this work can be written as

$$\mathcal{L}_{K_2^* N \Lambda^*} = i \frac{f_{K_2^* N \Lambda^*}}{m_{K_2^*}} \bar{\Lambda}^*_{\alpha} (g^{\alpha\mu} \partial^{\nu} + g^{\alpha\nu} \partial^{\mu}) N K_{2\mu\nu}^* \quad (8)$$

and the Reggeized amplitude for the K_2^* exchange is given by

$$i\mathcal{M}_{K_2^*} = -i \frac{2g_{\gamma K K_2^*}}{m_0^2} \frac{f_{K_2^* N \Lambda^*}}{m_{K_2^*}} \epsilon^{\alpha\beta\mu\lambda} \epsilon_{\mu} k_{\lambda} Q_{\alpha} q_{\rho} \Pi^{\beta\rho;\sigma\xi}(Q) \times \bar{u}^{\nu}(p') (g_{\nu\sigma} P_{\xi} + g_{\nu\xi} P_{\sigma}) u(p) \mathcal{R}^{K_2^*}(s, t) e^{-i\pi\alpha_{K_2^*}(t)}, \quad (9)$$

with the momentum $P = (p + p')/2$, and $\Pi^{\beta\rho;\sigma\xi}(q)$ the spin-2 projection given in Ref. [17].

The coupling constant $f_{K N \Lambda^*}$ is estimated to be $f_{K N \Lambda^*} = 10.59$ from the measured decay width $\Gamma_{\Lambda^* \rightarrow \bar{N} K} = 7.02$ MeV in the Particle Data Group.

The radiative decay constant in the K^* exchange is estimated to be $g_{\gamma K^+ K^{*+}} = \pm 0.254$ from the measured widths $\Gamma_{K^* \rightarrow \gamma K^{\pm}} = (0.05 \pm 0.005)$ MeV, and we take the negative sign to agree with empirical data. As mentioned before, however the determination of the coupling constant $f_{K^* N \Lambda^*}$ is still at large. We found in Ref. [7] that the phenomenological determination of the $K^* N \Lambda^*$ coupling constant was discussed rather in detail, in which case $g_{K^* N \Lambda^*} = \alpha_{\Lambda^*} g_{K N \Lambda^*}$ was assumed with the parameter $\alpha_{\Lambda^*} = +0.372$, or -0.657 obtained from the fit of the LAMP2 data [7]. By the different definition of the coupling vertex in the present work these correspond to $f_{K^* N \Lambda^*} = +7.12$ and -12.57 , respectively. But we note that the values of the α_{Λ^*} were determined by using the K^* -trajectory $\alpha_{K^*}(t) = 0.9t - 0.1$ and the energy-dependence of the Regge-pole $\sim s^{\alpha_{K^*}(t)}$, which are quite different from those we have employed in the present calculation. Moreover, such a lower intercept of the trajectory significantly reduces the contribution of the Regge-pole exchange so that a large coupling constant might be needed in their analysis in order for an agreement with the LAMP2 data.

In this work we consider to determine the $f_{K^* N \Lambda^*}$ from the numerical analysis of the reaction. Within the present framework, however, it is not a free parameter because it is related with coupling constant of the tensor meson K_2^* as

$$\frac{f_{K_2^* N \Lambda^*}}{m_{K_2^*}} = -3 \frac{f_{K^* N \Lambda^*}}{m_{K^*}} \quad (10)$$

by the duality and vector dominance [20]. Since the latter exchange is expected to play the role significant in the high energy region, we first obtain the K_2^* coupling constant as $-3f_{K^* N \Lambda^*}/m_{K^*} = -10.5/m_{K^*}$ by fitting to the SLAC data point at $E_{\gamma} = 11$ GeV, and then, the

TABLE I. Coupling constants of exchanged mesons in $\Lambda^*(1520)$ process. The meson-baryon coupling constants in the set I are for the CLAS and LEPS data and the set II for the LAMP2 and SLAC data. The signs of radiate decay constants $g_{\gamma K K^*} = -0.254$ and $g_{\gamma K K_2^*} = -0.276$ are taken in this work. The quark model prediction for $f_{K N \Lambda^*} \simeq 10$.

	Refs. [12, 13]	Ref. [7]	Set I	Set II
$f_{K N \Lambda^*}/\sqrt{4\pi}$	-0.15	2.99	1.8	2.5
$f_{K^* N \Lambda^*}$	± 1.58	-12.57, 7.12	3.5	3.5
$\frac{f_{K_2^* N \Lambda^*}}{m_{K_2^*}}$	-	-	$-\frac{10.5}{m_{K^*}}$	$-\frac{10.5}{m_{K^*}}$

$f_{K^* N \Lambda^*}$ is determined according to the relation in Eq. (10) above. We adopt these coupling constants in the case of spin-3/2 baryon of negative parity, because the duality and the vector dominance are believed to be universal. The radiative coupling constant for the K_2^* is estimated to be $g_{\gamma K K_2^*} = \pm 0.276$ from the decay width $\Gamma_{K_2^* \rightarrow \gamma K^{\pm}} = (0.24 \pm 0.05)$ MeV [21]. In the calculation we choose the negative sign for a better agreement with existing data.

The coupling constants for the present calculation are summarized in Table I and compared to those used for other model calculations.

As to the trajectory and phase of the t -channel Regge pole, we use

$$\begin{aligned} \alpha_K(t) &= 0.7(t - m_K^2), \\ \alpha_{K^*}(t) &= 0.83t + 0.25, \\ \alpha_{K_2^*}(t) &= 0.83(t - m_{K_2^*}^2) + 2, \end{aligned} \quad (11)$$

for a consistency with the previous works [17, 21, 22], and assign the complex phase to all the mesons K , K^* , and K_2^* as shown above.

III. NUMERICAL RESULTS

In this section we first discuss our result in the differential cross sections from the LAMP2 and SLAC experiment to examine the convergence of the reaction at high energies. Then, we present the cross sections from the CLAS and LEPS data in the lower energy region with the relevance of the coupling constants to the old and recent measurements indicated in Table I.

In order to avoid confusion in expression in what follows, we denote the symbol K by the single K exchange in Eq. (2) which is Reggeized by multiplying $(t - m_K^2) \mathcal{R}^K e^{-i\pi\alpha_K}$. Similarly, the symbols K^* and K_2^* denote the amplitudes in Eqs. (7) and (9) for brevity. Also we call the contact term to imply the amplitude in Eq. (3) without $M_{t(K)}$ and $M_{s(p)}$.

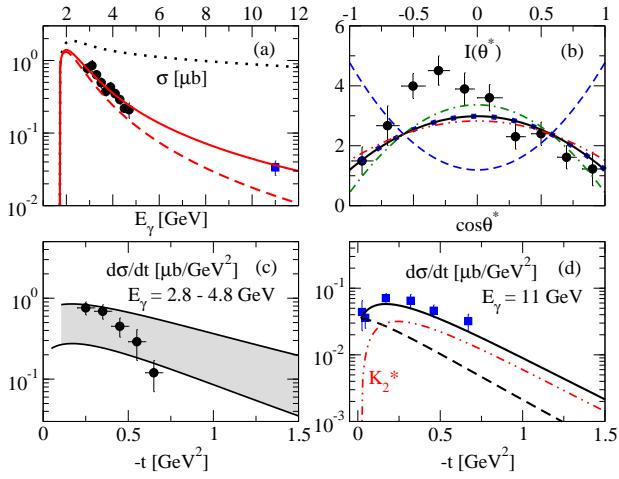


FIG. 2. Total and differential cross sections in (a) and (c) at $E_\gamma=2.8 \sim 4.8$ GeV [5], and the angular distribution of K^- in the decay $\Lambda^* \rightarrow K^- p$ in (b) from the LAMP2 measurement. The differential cross section from the SLAC at $E_\gamma = 11$ GeV is shown in (d) [6]. The dotted line in (a) results from the proton-pole with the charge term, $e_p(\not{p} + \not{k} + M_p)\not{\epsilon}$ in Eq. (4) for the full amplitude in Eq. (1). The cross sections without K_2^* are shown by the dashed lines in the total (a) and differential cross sections (d). In (b) the decay angle of K^- is denoted by θ^* for a distinction from the reaction angle θ of the K^+ produced. The $I(\theta^*)$ is reproduced at $E_\gamma = 3.8$ GeV and $\theta = 1^\circ$ by the density matrix elements ρ_{33} and ρ_{11} in Fig. 3 with the factor of 30 multiplied to Eq. (12). The contributions of K , K^* , and K_2^* are depicted by the blue dashed, green dash-dotted, red dash-dot-dotted line, in order. The blue dotted line is from the contact term and exactly coincides with the solid line from the full calculation. Note that the contribution of the K exchange from Eq. (2) is zero at $\theta = 0^\circ$ in (b).

A. Reaction at high energies

Before the LEPS and CLAS experiments [1–3] theoretical studies [7, 19] on this reaction had been based on the LAMP2 and SLAC data which were shown in Fig. 2 for the total, differential and the angular distribution of K^- in the decay $\Lambda^* \rightarrow K^- p$ in the final state.

In Fig. 2 the LAMP2 data for the total and differential cross sections at $E_\gamma = 2.8 \sim 4.8$ GeV and the SLAC differential cross section at $E_\gamma = 11$ GeV are reproduced by the full amplitude in Eq. (1) with the coupling constants from the set II in Table I. The leading coupling constant $f_{KN\Lambda^*}$ taken here is smaller than the value estimated from the measured decay width by a factor of 0.84. In order to test the validity of the minimal gauge we reproduce the total cross section with the charge term taken as $e_p(\not{p} + \not{k} + M_p)\not{\epsilon}$ in the proton-pole instead of $e_p 2p \cdot \epsilon$ in Eq. (4) and show the result by the dotted line in (a). This demonstrates that such a good convergence of the cross section to the experimental data cannot be obtained without the cutoff function, otherwise. Also it should be noted that the role of the K_2^* is crucial to re-

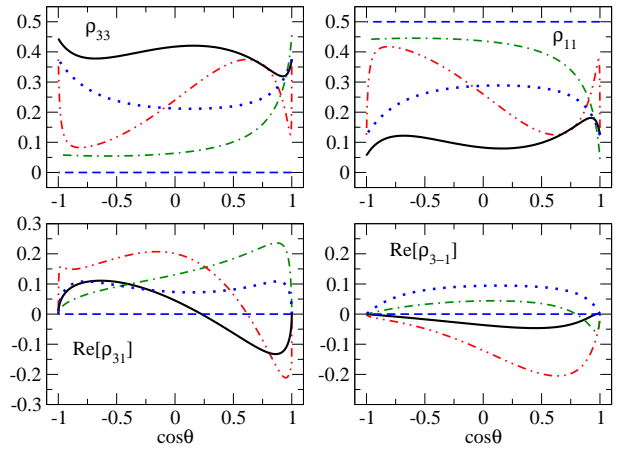


FIG. 3. Density matrix elements for the $\gamma p \rightarrow K^+ \Lambda^*$ at $E_\gamma = 3.8$ GeV. The angle θ dependence of the $\rho_{\lambda\lambda'}$ is calculated in the t -channel helicity frame of Λ^* [2, 14, 23]. Solid lines are the full calculation of the $\rho_{\lambda\lambda'}$ from the set II with the conventions and definitions from Refs. [24]. The respective contributions of K , K^* , and K_2^* are shown by the blue dashed, green dash-dotted, red dash-dot-dotted curves in order. The blue dotted line is from the contact term. The density matrix elements unravel the overall dependence of the $I(\theta^*)$ on the angle. At the $\theta = 0^\circ$, $\rho_{33} = 0.375$ and $\rho_{11} = 0.125$, respectively, to satisfy the trace condition $\rho_{33} + \rho_{11} = 1/2$.

produce the total and differential cross sections at high energy, as can be seen by comparing the solid lines with the dashed ones in (a) and (d).

The final state $\Lambda^*(1520)$ of spin-parity $3/2^-$ decaying to $K^- p$ system was measured in the LAMP2 group where the angular distribution of the K^- is given by

$$I(\theta^*) = \frac{3}{4\pi} \left[\rho_{33} \sin^2 \theta^* + \rho_{11} \left(\frac{1}{3} + \cos^2 \theta^* \right) \right], \quad (12)$$

with the angle θ^* of the decaying K^- in the Λ^* rest frame. Here, we neglect the remnants in the original equation in Ref. [5] by fixing the angle $\phi^* = 90^\circ$ as well as the smallness of the density matrix $\text{Re}[\rho_{3-1}]$ for simplicity. Since the dynamics of the photoproduction process is contained in the density matrix elements ρ_{33} and ρ_{11} , their dependences on the energy and angle are important to analyze the $I(\theta^*)$ in conjunction with the reaction mechanism of photoproduction.

In the photoproduction process associated with the decay channel, $\gamma p \rightarrow K^+ \Lambda^* \rightarrow K^+ K^- p$, the LAMP2 data was understood as the dominance of the Λ^* decay with the helicity $S_z = \pm 3/2$, as shown in Fig. 2 (b) where the K^* exchange of the natural parity in the photoproduction leads to the decay of the Λ^* with helicity $S_z = \pm 3/2$, which corresponds to the term of $\sin^2 \theta^*$, whereas the K exchange of unnatural parity to the $S_z = \pm 1/2$ corresponding to the term of $(\frac{1}{3} + \cos^2 \theta^*)$.

Figure 3 shows the density matrix elements ρ_{33} and ρ_{11} calculated in the t -channel helicity frame of Λ^* where the z -axis is taken to be the direction opposite to the

target proton momentum [2, 14, 23], as presented in the Appendix. At the $\theta \approx 0^\circ$ and at $E_\gamma = 3.8$ GeV, together with the small negative values for the $\text{Re}[\rho_{32}]$ and $\text{Re}[\rho_{3-1}]$, we obtain $\rho_{33} = 0.375$ and $\rho_{11} = 0.125$, which are consistent with those extracted from the LAMP2 data given in Table 1 of Ref. [5]. As the representative of each term in Eq. (12), therefore, the angular dependence of the $\rho_{\lambda\lambda'}$ in Fig. 3 can tell us that the ρ_{33} is always dominant as compared to the ρ_{11} in the overall range of the angle at the given energy. Thus, we expect the dominance of the natural parity exchange in the photoproduction from the shape of the $I(\theta^*)$ convex up and this is consistent with the LAMP2 data as we reproduced in Fig. 2 (b).

Within the present framework which is valid for the forward angles the dominance of the $\sin^2\theta$ term is due to the contribution of the contact term which dominates the photoproduction below $E_\gamma \approx 4$ GeV as shown in Fig. 4 in addition to the contributions of the $K^* + K_2^*$ at the very forward angle. As can be seen in Fig. 3, however, the contribution of the K_2^* is varying very rapidly near $\theta = 0^\circ$ in shaping the $I(\theta^*)$. Nevertheless, we find that the K exchange always yields the shape concave down by the role solely in the ρ_{11} .

Differential cross sections at $E_\gamma = 3.8 \pm 1$ GeV from the LAMP2 and 11 GeV from the SLAC experiments are presented in Fig. 3 (c) and (d). As shown by the dash-dot-dotted line in the latter case, the role of the K_2^* is apparent, and the dashed line in (d) as well as in (a) without it cannot agree with the experimental data for the differential and the total cross sections.

B. Reaction at low and in the intermediate energy

We now turn to the analysis of the experimental data recently measured by the CLAS and LEPS Collaborations.

Figure 4 shows the total cross section from the set I in Table I and the result is compared with the CLAS data. The dashed line of the LAMP2 cross section in Fig. 2 is also reproduced for comparison. Note that the discrepancy between the two, and we use the $f_{KN\Lambda^*}/\sqrt{4\pi} = 1.8$ in order to agree with new data. The dominance of the contact term over the meson exchanges in the CLAS data is illustrated. It should be pointed out that the exchange of the K_2^* as the natural parity becomes the leading contribution at high energy $E_\gamma = 11$ GeV to meet with the SLAC data. In contrast, the role of the K^* exchange is very small in comparison to those of K and K_2^* as shown in Fig. 4. This may explain why the cross sections is not sensitive to such a wide change of $K^*N\Lambda^*$ from 0 to ± 11 in the model without the tensor meson K_2^* [8].

Together with the total cross section in Fig. 4 the differential cross sections displayed in Fig. 5 shows that the reaction mechanism is feature by the leading role of the contact term followed by the K and K_2^* with equal contributions, and this feature from the CLAS measurement

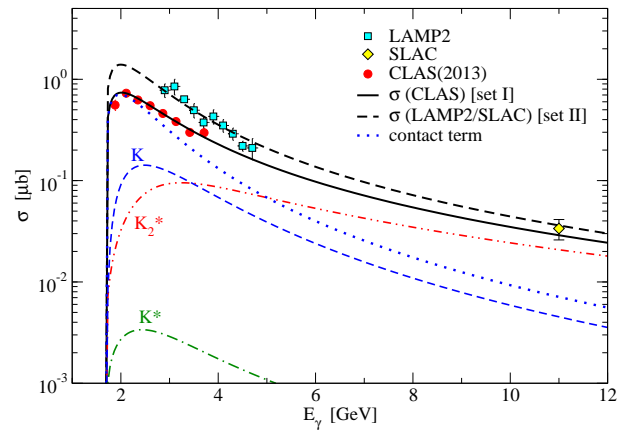


FIG. 4. Total cross sections for $\gamma p \rightarrow K^+ \Lambda^*(1520)$. Solid line is the full calculation of the cross section from the CLAS data with coupling constants set I in Table I. The dashed line is the total cross section of the LAMP2 and SLAC data with coupling constants of set II. The contributions of the contact term and the meson exchanges are shown with the same notations as in Fig. 3. The CLAS Data are taken from Ref. [1].

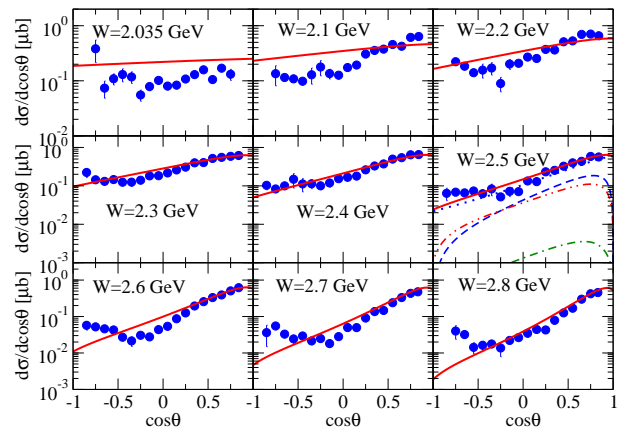


FIG. 5. Differential cross sections of the CLAS Collaboration in the nine energy bins. The solid line results from physical constants of the set I. The leading role of the contact term with the K and K_2^* following with equal contributions are well reproduced in the differential cross sections as well as the total cross section above. The contribution of meson exchange and the contact term are displayed with the same notations as in Fig. 4. Data are taken from Ref. [1].

is also valid for the differential cross sections measured in the LEPS experiment as will be shown in Fig. 6 next.

Shown in Figs. 6 and 7 are the energy and angle dependences of the differential cross sections and the energy dependence of the beam polarization asymmetry measured in a sequential experiment of the LEPS Collaboration. The roles of the contact term and each meson exchange discussed in the CLAS data are realized in these differ-

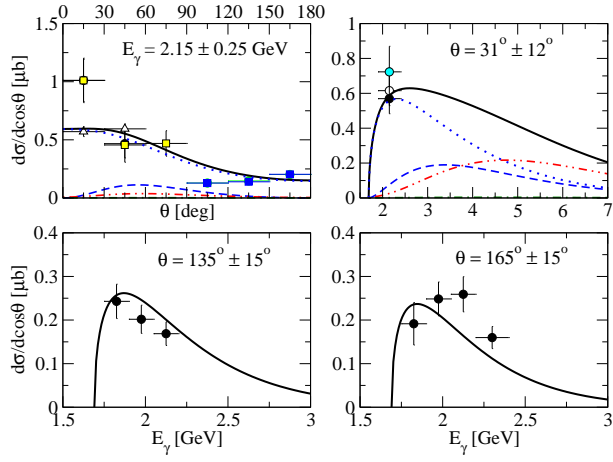


FIG. 6. Angle and energy dependences of differential cross sections measured in the range of the energy $1.9 < E_\gamma < 2.4$ GeV and the reaction angle $30 < \theta < 180$. The solid lines from the set I show the results at the central values in the experimental ranges. The contribution of meson exchange and the contact term are displayed with the same notations as in Fig. 4. Data of the LEPS in 2009 (black filled circle) are taken from Ref. [2].

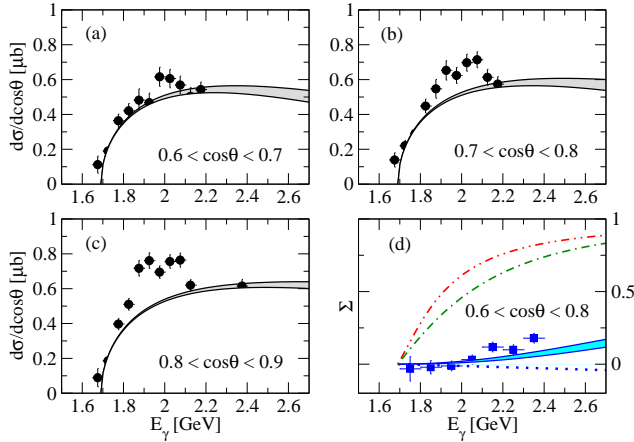


FIG. 7. Energy dependence of differential cross sections and beam polarization asymmetry measured in angle bins. The bands correspond to the cross sections in the range of angles denoted in each figure with coupling constants from the set I. The contribution of meson exchange and the contact term are displayed in the Σ with the same notations as in Fig. 4. Data of the LEPS in 2010 are taken from Ref. [3].

ential cross sections as well with respect to energy and angle, as shown in Fig. 6. Therefore, such a consistency of the LEPS data with the CLAS confirms the validity of the present analysis based on the Reggeized framework without fit parameters. However, the lack of the present model predictions in the backward region of the CLAS data in Fig. 5 as well as in the threshold peaks in the LEPS as shown in Fig. 7 (a), (b), (c) is suggestive of the contributions from the baryon resonances to the re-

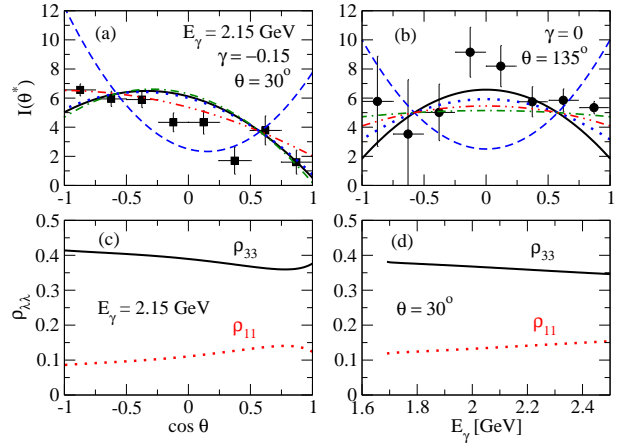


FIG. 8. Angular distributions of the polar K^- in the t -channel helicity frame of Λ^* . Solid curves are our results in the $I(\theta^*)$ from the set I with the parameters α and β replaced by ρ_{33} and ρ_{11} in Eq. (13). The solid curves in the forward (a) and backward (b) directions are estimated at $\theta = 30^\circ$ with $\gamma = -0.15$, and at $\theta = 135^\circ$ with $\gamma = 0$ for the fixed $N = 15$ at $E_\gamma = 2.15$ GeV. The contributions of the K , K^* , K_2^* , and the contact term are shown with the same notations as in Fig. 3. Data are taken from Ref. [2]. The angle and energy dependences of the ρ_{33} and ρ_{11} at forward angle (a) are presented by solid and dotted lines in (c) and (d).

action process. The LEPS data in 2009 [2] reported that $\Sigma \simeq -0.01 \pm 0.07$ at the kaon angle θ less than 60° in the energy interval $E_\gamma = 1.75 \sim 2.4$ GeV, and suggested that it is almost zero within the experimental uncertainties. The data from the LEPS in 2010 [3] showed a slightly positive value of Σ in the same energy range but for the different angles $0.6 < \cos\theta < 1$, and we reproduce it in the range of the angle $0.6 \leq \cos\theta \leq 0.8$ by using $\Sigma = \frac{d\sigma_y - d\sigma_x}{d\sigma_y + d\sigma_x}$, where x and y are the axes of the reaction plane perpendicular to the z -axis taken to be the incident photon momentum, as usual. The result presented in Fig. 7 (d) shows the large positive contributions from the $K^* + K_2^*$ of the natural parity and the large negative contribution of the K exchange, i.e., -1 , to the Σ , though not shown here. Hence the difference between the natural and unnatural parity leads to the positiveness of the Σ .

Finally, we reexamine the K^- angular distribution $I(\theta^*)$ in the Λ^* rest frame by using the LEPS measurement. The data were obtained by using a fit of K^+p mode based on the function,

$$I(\theta^*) = N \left[\alpha \sin^2 \theta^* + \beta \left(\frac{1}{3} + \cos^2 \theta^* \right) + \gamma \cos \theta^* \right], \quad (13)$$

where the effect of the background is further assumed in the last term with the parameter γ and a scale constant N to the arbitrary dimension of $I(\theta^*)$. The fractions of the Λ^* helicities $\pm 3/2$ and $\pm 1/2$ are parameterized as α and β , which were extracted to be about 0.52 and

0.48 from the LEPS fitting procedure in the kinematical ranges $1.9 < E_\gamma < 2.4$ GeV and $0^\circ < \theta < 60^\circ$. In the backward region the fractions $\alpha \approx 0.63$ and $\beta \approx 0.37$ were extracted in the angle $90^\circ < \theta < 180^\circ$ and energy range $1.7 < E_\gamma < 2.4$ GeV. Here, we consider to recover the α and β as the ρ_{33} and ρ_{11} , as before, in order to give them the energy and angle dependences in Eq. (13). Given the constant $N = 15$, we obtain those solid curves in Fig. 8 with $\gamma = -0.15$ at $\theta = 30^\circ$ for the forward (a) and $\gamma = 0$ at $\theta = 135^\circ$ for the backward (b) directions at $E_\gamma = 2.15$ GeV by using the ρ_{33} and ρ_{11} calculated in the t -channel helicity frame at the given energy and angles.

In order to examine the variation of the $I(\theta^*)$ at the central values of angle and energy as in (a) and (b) within the experimental ranges of angle and energy, we calculate the angle and energy dependences of the ρ_{33} and ρ_{11} to confirm that the variations of these variables are not significant as shown in (c) and (d). Furthermore, the overall dominance of the ρ_{33} over the ρ_{11} is apparent in the given ranges of angle and energy. Thus, we compare $\rho_{33} \approx 0.38$ and $\rho_{11} \approx 0.12$ to those $\alpha/2 \approx 0.26$ and $\beta/2 \approx 0.24$ from the fit of the LEPS above at forward angle, by considering that the trace condition of the latter is twice that of the former. This supports the result in the analysis of the LAMP2 data.

IV. SUMMARY AND DISCUSSION

In this work we have investigated the reaction $\gamma p \rightarrow K^+ \Lambda^*(1520)$ from threshold to photon energy $E_\gamma = 11$ GeV based on the production amplitude in Eq. (1) for the meson exchanges in the t -channel. Following the convention and definitions of the previous works [17, 21, 22] the t -channel exchanges are Reggeized with the trajectories taken the same as those $\gamma p \rightarrow K^+ \Lambda$, $\gamma p \rightarrow K^{*+} \Lambda$, and $\gamma p \rightarrow K^+ \Sigma^*(1385)$ for consistency's sake.

Covering whole range of the reaction energy for the CLAS, LEPS, LAMP2 and SLAC experiments the cross sections for total, differential, and beam polarization asymmetry are analyzed without either cutoff functions or fit-parameters. The angular distribution of the K^- from the $\Lambda^* \rightarrow K^- p$ decay in the final state is discussed based on the role of the density matrix elements played in the LAMP2 and LEPS data. The basic ingredients of this simple model are the minimal gauge prescription for the convergence of the reaction to the experimental data and the role of the K_2^* substantial to agree with data at high energies. Within the present framework, therefore, the electromagnetic production of spin-3/2 baryon resonance of negative parity could simply be understood as the production mechanism similar to the well-known cases of $\pi \Delta$ [15] and $K \Sigma^*$ [17], just as we have illustrated here.

Through out the analysis of the total and differential cross sections we find that the production mechanism is featured by the dominance of the contact term and the K

and K_2^* exchanges follow with almost equal contributions in the low energy region. While the role of the K^* exchange is minor, the K_2^* exchange plays the role leading over other exchanges in the reaction process at high energies. Though determined from the phenomenological analysis, here, the coupling constant of $f_{K^* N \Lambda^*} = 3.5$ is interesting because it is closer to the result of the $\bar{K} N$ coupled channel approach [13] rather than the quark model prediction. It should be recalled that the determination of the K^* in this work is not a free parameter but bound to a determination of the K_2^* coupling constant by Eq. (10), which is set to agree with the SLAC data at $E_\gamma = 11$ GeV. Therefore, the difficulty in identifying the coupling strength of the K^* in previous studies is resolved by including the K_2^* with both coupling constants set to be determined simultaneously in one relation.

Based on the density matrix elements presented here, we analyze the angular distribution function $I(\theta^*)$ for the $\Lambda^* \rightarrow K^- p$ decay to investigate the role of the natural and unnatural parity exchanges in the photoproduction process. By using the t -channel helicity frame of Λ^* for the calculation of the density matrix elements $\rho_{\lambda\lambda'}$, we show that the numerical analysis of the LAMP2 and LEPS data on the $I(\theta^*)$ is consistent with the dominance of the helicity $\pm 3/2$ of Λ^* decay due to the strong contribution of the ρ_{33} by the contact term in addition to the $K^* + K_2^*$ contributions. This finding is, however, contradictory to the experiments in the SAPHIR [4] and the CLAS albeit the latter case of electroproduction has more reasons to be [14]. Therefore, such a contradiction in explaining the $I(\theta^*)$ should be clarified in experiments by the precise measurements of the ρ_{33} and ρ_{11} in a specified G.-J. frame.

As an application of the present work it is desirable to reexamine the N^* resonances here because the role of K_2^* as a new entry to the process is expected to regularize the χ^2 -fit to some degree with a hope that the double-counting by the duality between s - and t -channels should not be significant from the smallness of the N^* contribution expected.

ACKNOWLEDGMENT

The authors are grateful to S.-i. Nam for fruitful discussions about the present work. This work was supported by the grant NRF-2013R1A1A2010504, and by the grant NRF-2016K1A3A7A09005580 from National Research Foundation (NRF) of Korea.

Appendix A: Density matrix in t -channel helicity frame of Λ^*

We calculate the density matrix elements using the helicity formalism in the Gottfried-Jackson (G.-J.) frame where the Λ^* is rest. The z -axis can be taken either as the direction of the incident photon or as the tar-

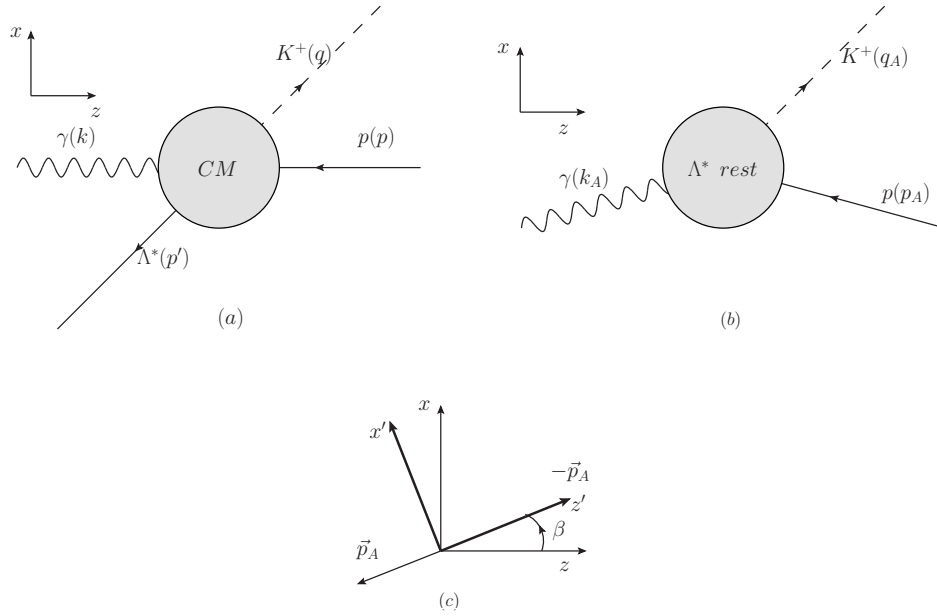


FIG. 9. Photoproduction in the c.m. frame (a), and in the Λ^* rest frame called as the Adair frame (b). The rotation from the Adair to the t -channel helicity frame of Λ^* by the angle β (c).

get proton in the Λ^* rest frame conventionally, while the y -axis is defined to be normal to the production plane, i.e., $\hat{y} \propto \hat{\gamma} \times \hat{K}^+$. In the present calculation, we take the z -axis to be antiparallel to the direction of the target proton following the Ref. [14], which is called the t -channel helicity frame of Λ^* . To work with the Helicity formalism, we perform the Lorentz transformation of the kinematic variables k, q, p, p' (which are the respective momenta of the photon, K^+ , proton, and Λ^*) from the center of mass frame to the Λ^* rest frame. By doing this the boosted momenta k_A, q_A, p_A, p'_A are obtained in the Λ^* rest frame, the so-called the Adair frame. Then, we construct the helicity eigenstate for each momentum in the Adair frame.

For the target proton with mass M_p , we use the helicity solutions as follows,

$$\psi(p_A, \frac{1}{2}) = N \begin{pmatrix} \cos \frac{\theta}{2} \\ e^{i\phi} \sin \frac{\theta}{2} \\ \frac{|\vec{p}_A|}{E+M_p} \cos \frac{\theta}{2} \\ \frac{|\vec{p}_A|}{E+M_p} e^{i\phi} \sin \frac{\theta}{2} \end{pmatrix}, \quad (\text{A1})$$

$$\psi(p_A, -\frac{1}{2}) = N \begin{pmatrix} -\sin \frac{\theta}{2} \\ e^{i\phi} \cos \frac{\theta}{2} \\ \frac{|\vec{p}_A|}{E+M_p} \sin \frac{\theta}{2} \\ -\frac{|\vec{p}_A|}{E+M_p} e^{i\phi} \cos \frac{\theta}{2} \end{pmatrix}, \quad (\text{A2})$$

where $p_A = (E, |\vec{p}_A| \sin \theta \cos \phi, |\vec{p}_A| \sin \theta \sin \phi, |\vec{p}_A| \cos \theta)$ is the momentum of target proton in the Adair frame and N is the normalization constant.

For the Λ^* resonance, the Rarita-Schwinger field of spin-3/2 baryon is constructed from the vector-spinor

representation

$$\begin{aligned} \psi^\mu(p, \frac{3}{2}) &= \epsilon_+^\mu(p) u(p, \frac{1}{2}), \\ \psi^\mu(p, \frac{1}{2}) &= \sqrt{\frac{2}{3}} \epsilon_0^\mu(p) u(p, \frac{1}{2}) + \sqrt{\frac{1}{3}} \epsilon_+^\mu(p) u(p, -\frac{1}{2}), \\ \psi^\mu(p, -\frac{1}{2}) &= \sqrt{\frac{1}{3}} \epsilon_-^\mu(p) u(p, \frac{1}{2}) + \sqrt{\frac{2}{3}} \epsilon_0^\mu(p) u(p, -\frac{1}{2}), \\ \psi^\mu(p, -\frac{3}{2}) &= \epsilon_-^\mu(p) u(p, -\frac{1}{2}), \end{aligned} \quad (\text{A3})$$

where $p = (M_{\Lambda^*}, 0, 0, 0)$, and M_{Λ^*} is the mass of the Λ^* . For the spinor $u(p)$, the following wave functions are used

$$u(p, \frac{1}{2}) = \begin{pmatrix} 1 \\ 0 \\ 0 \\ 0 \end{pmatrix}, \quad (\text{A4})$$

$$u(p, -\frac{1}{2}) = \begin{pmatrix} 0 \\ 1 \\ 0 \\ 0 \end{pmatrix}. \quad (\text{A5})$$

For the vector $\epsilon^\mu(p)$, the following helicity wave functions are used

$$\epsilon_\pm^\mu(p) = \frac{1}{\sqrt{2}}(0, \mp 1, -i, 0), \quad (\text{A6})$$

$$\epsilon_0^\mu(p) = (0, 0, 0, 1). \quad (\text{A7})$$

Once we get the density matrix elements ρ_A in the Adair frame, we need to perform the coordinate transformation once more from the Adair to the G.-J. frame to obtain the ρ_{GJ} there. In other words, to go to the G.-J. frame where the z -axis is antiparallel to the incident proton direction, we need to rotate the ρ_A about y -axis using the Wigner rotation matrix, i.e.,

$$\rho_{GJ} = d^\dagger(\beta)\rho_A d(\beta). \quad (\text{A8})$$

Here the β is the angle of the rotation between the incident proton direction and the z -axis in the Adair frame as shown in Fig. 9. We summarize the procedure discussed above in a diagrammatic representation in Fig. 9.

Appendix B: Angular distribution function for $\Lambda^* \rightarrow K^- p$

The angular distribution function $W(\theta, \phi)$ for $\Lambda^* \rightarrow K^- p$ decay measures the decay angle (θ, ϕ) of K^- in the

G.-J. frame (the same angles (θ^*, ϕ^*) in the text) with respect to the incident photon polarization;

$$\vec{P}_\gamma = P_\gamma (-\cos 2\Phi, -\sin 2\Phi, 0), \quad (\text{B1})$$

where Φ is the angle between the polarization vector of the photon and reaction plane, and

$$W(\theta, \phi, \Phi) = W^0(\theta, \phi) + \sum_{i=1}^3 P_\gamma^i(\Phi) W^i(\theta, \phi). \quad (\text{B2})$$

The angular distribution function W^α for $\alpha = 0, 1, 2, 3$ is expressed in terms of the density matrix elements as [25]

$$W^\alpha(\theta, \phi) = \frac{2J+1}{8\pi} \sum_{\lambda''} D_{\lambda\lambda''}^{(3/2)*}(\phi, \theta, -\phi) \rho_{\lambda\lambda''}^\alpha D_{\lambda'\lambda''}^{(3/2)}(\phi, \theta, -\phi) \quad (\text{B3})$$

for the decay of $\text{spin-}\frac{3}{2} \rightarrow \text{spin-0} + \text{spin-}\frac{1}{2}$ with $\lambda'' = +\frac{1}{2}$, or $-\frac{1}{2}$, i.e.,

$$W^\alpha(\theta, \phi) = \frac{1}{2\pi} \left[D_{\lambda\frac{1}{2}}^{(3/2)*}(\phi, \theta, -\phi) \rho_{\lambda\lambda'}^\alpha D_{\lambda'\frac{1}{2}}^{(3/2)}(\phi, \theta, -\phi) + D_{\lambda-\frac{1}{2}}^{(3/2)*}(\phi, \theta, -\phi) \rho_{\lambda\lambda'}^\alpha D_{\lambda'-\frac{1}{2}}^{(3/2)}(\phi, \theta, -\phi) \right] \quad (\text{B4})$$

with the $\text{spin-}\frac{3}{2}$ rotation matrix elements given by

$$D_{\lambda\frac{1}{2}}^{(3/2)} = \left(-\sqrt{3} \cos^2 \frac{\theta}{2} \sin \frac{\theta}{2} e^{-i\phi}, \cos^3 \frac{\theta}{2} - 2 \cos \frac{\theta}{2} \sin^2 \frac{\theta}{2}, (2 \cos^2 \frac{\theta}{2} \sin \frac{\theta}{2} - \sin^3 \frac{\theta}{2}) e^{i\phi}, \sqrt{3} \cos \frac{\theta}{2} \sin^2 \frac{\theta}{2} e^{2i\phi} \right), \quad (\text{B5})$$

$$D_{\lambda-\frac{1}{2}}^{(3/2)} = \left(\sqrt{3} \cos \frac{\theta}{2} \sin^2 \frac{\theta}{2} e^{-2i\phi}, (\sin^3 \frac{\theta}{2} - 2 \cos^2 \frac{\theta}{2} \sin \frac{\theta}{2}) e^{-i\phi}, -(2 \cos \frac{\theta}{2} \sin^2 \frac{\theta}{2} - \cos^3 \frac{\theta}{2}), \sqrt{3} \sin \frac{\theta}{2} \cos^2 \frac{\theta}{2} e^{i\phi} \right). \quad (\text{B6})$$

Here, the density matrix elements are

$$\rho_{\lambda\lambda'}^\alpha = \begin{pmatrix} \rho_{33} & \text{Re } \rho_{31} + i \text{Im } \rho_{31} & \text{Re } \rho_{3-1} + i \text{Im } \rho_{3-1} & i \text{Im } \rho_{3-3} \\ \text{Re } \rho_{31} - i \text{Im } \rho_{31} & \rho_{11} & i \text{Im } \rho_{1-1} & \text{Re } \rho_{3-1} - i \text{Im } \rho_{3-1} \\ \text{Re } \rho_{3-1} - i \text{Im } \rho_{3-1} & -i \text{Im } \rho_{1-1} & \rho_{11} & -\text{Re } \rho_{31} + i \text{Im } \rho_{31} \\ -i \text{Im } \rho_{3-3} & \text{Re } \rho_{3-1} + i \text{Im } \rho_{3-1} & -\text{Re } \rho_{31} - i \text{Im } \rho_{31} & \rho_{33} \end{pmatrix} \quad (\text{B7})$$

for $\alpha = 0, 1$ with $\text{Re } [\rho_{3-3}] = 0 = \text{Re } [\rho_{1-1}]$ by hermicity and parity, and

$$\rho_{\lambda\lambda'}^2 = \begin{pmatrix} \rho_{33} & \text{Re } \rho_{31} + i \text{Im } \rho_{31} & \text{Re } \rho_{3-1} + i \text{Im } \rho_{3-1} & \text{Re } \rho_{3-3} \\ \text{Re } \rho_{31} - i \text{Im } \rho_{31} & \rho_{11} & \text{Re } \rho_{1-1} & -\text{Re } \rho_{3-1} + i \text{Im } \rho_{3-1} \\ \text{Re } \rho_{3-1} - i \text{Im } \rho_{3-1} & \text{Re } \rho_{1-1} & -\rho_{11} & \text{Re } \rho_{31} - i \text{Im } \rho_{31} \\ \text{Re } \rho_{3-3} & -\text{Re } \rho_{3-1} - i \text{Im } \rho_{3-1} & \text{Re } \rho_{31} + i \text{Im } \rho_{31} & -\rho_{33} \end{pmatrix} \quad (\text{B8})$$

with $\text{Im } [\rho_{3-3}] = 0 = \text{Im } [\rho_{1-1}]$.

Thus, the angular distribution functions for $\alpha = 0, 1$ and $\alpha = 2$ are given by

$$W^\alpha(\theta, \phi) = \frac{3}{4\pi} \left[\rho_{33}^\alpha \sin^2 \theta + \rho_{11}^\alpha \left(\frac{1}{3} + \cos^2 \theta \right) - \frac{2}{\sqrt{3}} \text{Re } \rho_{31}^\alpha \sin 2\theta \cos \phi - \frac{2}{\sqrt{3}} \text{Re } \rho_{3-1}^\alpha \sin^2 \theta \cos 2\phi \right], \quad (\text{B9})$$

$$W^2(\theta, \phi) = \frac{3}{4\pi} \left(\frac{2}{\sqrt{3}} \text{Im } \rho_{31}^2 \sin 2\theta \sin \phi + \frac{2}{\sqrt{3}} \text{Im } \rho_{3-1}^2 \sin^2 \theta \sin 2\phi \right). \quad (\text{B10})$$

Therefore, according to Eq. (B2), the decay angular distribution in the G.-J. frame is given by [27]

$$\begin{aligned}
W(\theta, \phi, \Phi) = & \frac{3}{4\pi} \left\{ \rho_{33}^0 \sin^2 \theta + \rho_{11}^0 \left(\frac{1}{3} + \cos^2 \theta \right) - \frac{2}{\sqrt{3}} \text{Re} [\rho_{31}^0 \cos \phi \sin 2\theta + \rho_{3-1}^0 \cos 2\phi \sin^2 \theta] \right. \\
& - P_\gamma \cos 2\Phi \left[\rho_{33}^1 \sin^2 \theta + \rho_{11}^1 \left(\frac{1}{3} + \cos^2 \theta \right) - \frac{2}{\sqrt{3}} \text{Re} [\rho_{31}^1 \cos \phi \sin 2\theta + \rho_{3-1}^1 \cos 2\phi \sin^2 \theta] \right] \\
& \left. - P_\gamma \sin 2\Phi \frac{2}{\sqrt{3}} \text{Im} [\rho_{31}^2 \sin \phi \sin 2\theta + \rho_{3-1}^2 \sin 2\phi \sin^2 \theta] \right\}. \tag{B11}
\end{aligned}$$

The beam polarization asymmetry is defined by integrating the W over the θ, ϕ angles,

$$\Sigma = -\frac{1}{P_\gamma} \frac{W(\Phi = 0) - W(\Phi = \frac{\pi}{2})}{W(\Phi = 0) + W(\Phi = \frac{\pi}{2})} \tag{B12}$$

which leads to

$$\Sigma = 2(\rho_{33}^1 + \rho_{11}^1). \tag{B13}$$

And in relation with the multikaon process the beam polarization asymmetry Σ with the final kaon measured at the specific angles $\theta = 90^\circ$ and $\phi = 90^\circ$ in Eq. (B11)

is written as [26]

$$\begin{aligned}
\Sigma^* = & -\frac{1}{P_\gamma} \frac{W(\frac{\pi}{2}, \frac{\pi}{2}, \Phi = 0) - W(\frac{\pi}{2}, \frac{\pi}{2}, \Phi = \frac{\pi}{2})}{W(\frac{\pi}{2}, \frac{\pi}{2}, \Phi = 0) + W(\frac{\pi}{2}, \frac{\pi}{2}, \Phi = \frac{\pi}{2})}, \\
= & \frac{\rho_{33}^1 + \frac{1}{3}\rho_{00}^1 + \frac{2}{\sqrt{3}}\text{Re}[\rho_{3-1}^1]}{\rho_{33}^0 + \frac{1}{3}\rho_{00}^0 + \frac{2}{\sqrt{3}}\text{Re}[\rho_{3-1}^0]} \tag{B14}
\end{aligned}$$

for the measurement at the fixed angle θ, ϕ .

The Σ in Eqs. (B13) is equivalent to the beam polarization asymmetry

$$\Sigma = \frac{d\sigma_y - d\sigma_x}{d\sigma_y + d\sigma_x} \tag{B15}$$

defined in the center of mass frame. The estimate of the density matrix elements is in general dependent on the frame chosen for calculation.

-
- [1] K. Moriya *et al.*, Phys. Rev. C **88**, 045201 (2013).
[2] N. Muramatsu *et al.*, Phys. Rev. Lett. **103** 012001 (2009).
[3] H. Khorri *et al.*, Phys. Rev. Lett. **104**, 172001 (2010).
[4] F. W. Wieland *et al.*, Eur. Phys. J. A **47**, 47 (2011).
[5] D. P. Barber *et al.*, Z. Phys. C **7**, 17 (1980).
[6] A. M. Boyarski *et al.*, Phys. Lett. B **34**, 547 (1971).
[7] A. I. Titov, B. Kämpfer, S. Daté, and Y. Ohashi, Phys. Rev. C **72**, 035206 (2005).
[8] S.-i. Nam and C.-W. Kao, Phys. Rev. C **81**, 055206 (2010).
[9] J. He and X.-R. Chen, Phys. Rev. C **86** 035204 (2012).
[10] J.-J. Xie, E. Wang and J. Nieves, Phys. Rev. C **89**, 015203 (2014).
[11] E. Wang, J.-J. Xie and J. Nieves, Phys. Rev. C **90**, 065203 (2014).
[12] L. Roca, S. Sarkar, V. K. Magas, and E. Oset, Phys. Rev. C **73**, 045208 (2006).
[13] T. Hyodo, S. Sarkar, A. Hosaka, and E. Oset, Phys. Rev. C **73**, 035209 (2006).
[14] S. P. Barrow *et al.*, Phys. Rev. C **64** 044601 (2001).
[15] B.-G. Yu and K.-J. Kong, arXiv:1611.09629 [hep-ph].
[16] B.-G. Yu and K.-J. Kong, arXiv:1612.02071 [hep-ph].
[17] B.-G. Yu and K.-J. Kong, arXiv:1702.03674 [nucl-th].
[18] P. Stichel and M. Scholz, Nuovo Cimento **34**, 1381 (1964).
[19] H. Toki, C. García-Recio and J. Nieves, Phys. Rev. D **77**, 034001 (2008).
[20] G. Goldstein and J. F. Owens III, Nucl. Phys. B **71** 461 (1974).
[21] B.-G. Yu, T. K. Choi and W. Kim, Phys. Lett. B **701**, 332 (2011).
[22] B.-G. Yu, Y. Oh and K.-J. Kong, arXiv:1608.00455 [hep-ph].
[23] K. Schilling, P. Seyboth, and G. Wolf, Nucl. Phys. B **15**, 397 (1970).
[24] S. Donnachie, G. Dosch, P. Landshoff and O. Nachtmann, *Pomeron Physics and QCD*, Cambridge University Press (2002).
[25] S. U. Chung and T. L. Trueman, Phys. Rev. D **11**, 633 (1975).
[26] Qiang Zhao, Phys. Rev. C **632**, 0252039 (2001).
[27] H. H. Bingham *et al.*, Phys. Rev. Lett. **25**, 1223 (1970).